Relativistic L-shell Auger and Coster-Kronig rates and fluorescence yields

Mau Hsiung Chen, Ekaputra Laiman, and Bernd Crasemann
Department of Physics, University of Oregon, Eugene, Oregon 97403

Michio Aoyagi
Ames Research Center, National Aeronautics and Space Administration, Moffett Field, California 94035

Hans Mark
Department of the Air Force, Washington, D.C. 20330
(Received 11 December 1978)

Relativistic calculations of radiationless transition rates to L-subshell vacancy states in selected atoms with $70 \leq Z \leq 96$ have been performed. The Auger and Coster-Kronig transition probabilities are calculated from perturbation theory, assuming frozen orbitals, in the Dirac-Hartree-Slater approach. Transition rates, fluorescence yields, and Coster-Kronig yields are compared with nonrelativistic theoretical results and with experiment. Relativity is found to affect the L-subshell Auger widths by (10–25)% and individual transition rates to certain j-j configurations by as much as 40% at $Z = 80$. The widths of L_i vacancy states and the L_2 Coster-Kronig yields f_{23} from these relativistic calculations agree much better with experiment than earlier nonrelativistic theoretical values.

I. INTRODUCTION

Atomic inner-shell vacancies, with rare exceptions, are filled predominantly by radiationless transitions. Vacancy lifetimes are therefore determined, in general, by Auger and Coster-Kronig transition rates. Since the time when Wentzel formulated the basic ansatz for the calculation of Auger rates,[1] much theoretical work has been done on the subject, both for the derivation of theoretical x-ray fluorescence yields[2] and for the prediction and interpretation of Auger spectra and lifetimes of excited states.[3,4]

With few exceptions, theoretical work on Auger transitions has heretofore been confined to nonrelativistic calculations. The earliest attempt at a relativistic treatment is that of Massey and Burhop,[5] who used screened hydrogenic wave functions to deduce the K-LL rates of gold. Relativistic K-LL rates were calculated by Asaad[6] with numerical wave functions in a Hartree potential, and by Listengarten[7] in a Thomas-Fermi-Dirac potential. Bhalla and Ramsdale[8] have calculated selected K-LL, K-LM, K-MM, and the first six of the L_1-MM transition rates with Hartree-Fock-Slater wave functions. Chattarji and Talukdar[9] attempted to compute L_1 Coster-Kronig rates with screened hydrogenic wave functions. No successful relativistic calculations of other radiationless transitions have been performed to date, and no comprehensive and systematic calculations have been carried out. In this paper, we report on relativistic calculations of L-shell Auger and Coster-Kronig rates and fluorescence yields for selected elements in the range $70 \leq Z \leq 96$.

II. THEORY

We calculate the radiationless transition probability from perturbation theory. Frozen orbitals are assumed; in this approximation only the two-electron operator is involved in the process. In the nonrelativistic theory, this interaction is just the Coulomb repulsion between the two electrons.[2]

Earlier relativistic treatments of the Auger effect[5-8] we re based on Møller's formula,[10] obtained from the correspondence principle. The Auger transition probability can also be evaluated through the quantum-electrodynamic theory of the retarded interaction between two charges.[11,12]

From perturbation theory and in the active-electron approximation, the Auger transition probability in j-j coupling is

$$T(\alpha JM \to \alpha' J'M') = |D - E|^2 , \tag{1}$$

where α (α') stands for all quantum numbers other than J and M (J' and M') needed to identify the states.

The direct matrix element D and the exchange matrix element E are

$$D = \langle j_1'(1) j_2'(2) J'M' | V_{12} | j_1(1) j_2(2) JM \rangle , \tag{2}$$

$$E = \langle j_1'(1) j_2'(2) J'M' | V_{12} | j_1(2) j_2(1) JM \rangle . \tag{3}$$

The major component of the wave function of the initial hole is characterized by the quantum numbers n_1', l_1', j_1'; that of the continuum electron by n_2', l_2', j_2', and of the final holes by n_1, l_1, j_1, and n_2, l_2, j_2. In Eqs. (2) and (3), $|j_1'(1) j_2'(2) J'M'\rangle$ denotes the (not antisymmetrized) wave function of electron 1 in the state characterized by the quan-

tum number j_1' and electron 2 in the state characterized by j_2', coupled to total angular momentum quantum numbers $J'M'$. The continuum wave function is assumed to be normalized to represent one ejected electron per unit time.[6] Atomic units are used throughout in this paper.

There are several forms of the relativistic two-electron operator V_{12}, involving different degrees of approximation.[12,13] We choose the general form of V_{12} in the local approximation, as given by the original Møller formula

$$V_{12} = (1 - \vec{\alpha}_1 \cdot \vec{\alpha}_2)\exp(i\omega r_{12})/r_{12} . \tag{4}$$

This form of the operator includes the retarded Coulomb and current-current interactions. The $\vec{\alpha}_i$ are Dirac matrices. We have $\omega = |E_1' - E_1|/c$ in the direct matrix element [Eq. (2)], where E_1' is the eigenenergy of the state j_1' and E_1 is the eigenenergy of the state j_1. In the exchange matrix element [Eq. (3)], the corresponding relation is $\omega = |E_1' - E_2|/c$. Equation (4) represents the interaction V_{12} in a form suitable for electron orbitals in a local potential, as in the Dirac-Hartree-Slater model used here.

We only deal with atoms that contain one initial inner-shell vacancy, and we neglect the coupling between the inner-shell vacancy and the outermost open shell (if any) of the neutral atom. The orbital wave functions are assumed to satisfy a set of Dirac-Fock equations with a local exchange potential; they have the form[14]

$$\Psi_{n\kappa m}(r) = \frac{1}{r}\begin{pmatrix} G_{n\kappa}(r)\Omega_{\kappa m} \\ iF_{n\kappa}(r)\Omega_{-\kappa m}\end{pmatrix} , \tag{5}$$

where

$$\Omega_{\kappa m} = \sum_{\mu} C(\tfrac{1}{2}\, lj;\, \mu,\, m-\mu)Y_{l\mu}(\theta,\phi)\chi_{1/2,m-\mu} \tag{6a}$$

and

$$\Omega_{-\kappa m} = \sum_{\mu} C(\tfrac{1}{2}\, \bar{l}j;\, \mu,\, m-\mu)Y_{\bar{l}\mu}(\theta,\phi)\chi_{1/2,m-\mu} , \tag{6b}$$

with $\kappa = (l-j)(2j+1)$.

To evaluate the direct and exchange matrix elements, the retarded potential is separated into angular and radial parts by means of the expansion

$$\frac{e^{i\omega r_{12}}}{r_{12}} = \sum_{\lambda=0}^{\infty} \gamma_\lambda(r_1 r_2) C^\lambda(1)\cdot C^\lambda(2), \tag{7}$$

where

$$\gamma_\lambda(r_1 r_2) = -(2\lambda+1)\omega j_\lambda(\omega r_<)\mathcal{Y}_\lambda(\omega r_>) + i(2\lambda+1)\omega j_\lambda(\omega r_<) j_\lambda(\omega r_>), \tag{8}$$

and $r_<$ ($r_>$) is the smaller (larger) of r_1 and r_2. Here, j_λ and $\mathcal{Y}_\lambda$ are spherical Bessel functions of the first and second kind, respectively; C^λ is the spherical tensor. The direct matrix element can be written as a sum of two terms,

$$D = D' + D'', \tag{9}$$

where

$$D' = \langle j_1' j_2' J'M' | (1/r_{12}) e^{i\omega r_{12}} | j_1 j_2 JM\rangle \tag{10a}$$

and

$$D'' = -\langle j_1' j_2' J'M' | (1/r_{12}) e^{i\omega r_{12}} (\vec{\alpha}_1 \cdot \vec{\alpha}_2) | j_1 j_2 JM\rangle . \tag{10b}$$

Racah algebra is used to separate the matrix elements into angular parts multiplied by radial integrals. The term D' is easily obtained:

$$D' = \sum_{\lambda=0}^{\infty} (-1)^{j_2+j_2'+J}[j_1, j_1', j_2, j_2']^{1/2} \begin{Bmatrix} j_1' & j_2' & J \\ j_2 & j_1 & \lambda \end{Bmatrix} \begin{pmatrix} j_1' & j_1 & \lambda \\ -\frac{1}{2} & \frac{1}{2} & 0 \end{pmatrix} \begin{pmatrix} j_2' & j_2 & \lambda \\ -\frac{1}{2} & \frac{1}{2} & 0 \end{pmatrix} \times \Pi(l_1'\lambda l_1)\Pi(l_2'\lambda l_2)\langle W_{11}\gamma_\lambda W_{22}\rangle \delta_{JJ'}\delta_{MM'}, \tag{11}$$

where

$$\langle W_{11}\gamma_\lambda W_{22}\rangle = \int_0^\infty \int_0^\infty W_{11}(r_1)\gamma_\lambda(r_1 r_2) \times W_{22}(r_2)\, dr_1\, dr_2 , \tag{12}$$

with

$$W_{ij}(r) = G_i'(r)G_j(r) + F_i'(r)F_j(r) \tag{13}$$

and

$$\Pi(l'\lambda l) = \begin{cases} 1 \text{ if } l'+\lambda+l \text{ is even} \\ 0 \quad \text{otherwise} \end{cases} . \tag{14}$$

The quantity $[j_1, j_1', j_2, j_2', \dots]$ is defined as

$$[j_1, j_1', j_2, j_2', \dots]^{1/2} = [(2j_1+1)(2j_1'+1)(2j_2+1)(2j_2'+1)\cdots]^{1/2} . \tag{15}$$

By means of the relation[15]

$$\sum_\lambda (\vec{\alpha}_1 \cdot \vec{\alpha}_2)(C_1^\lambda \cdot C_2^\lambda)\gamma_\lambda(r_1 r_2) = \sum_\lambda \sum_{\mu=\lambda-1}^{\mu=\lambda+1} (\vec{\alpha}_1 \times C_1^\lambda)^\mu \cdot (\vec{\alpha}_2 \times C_2^\lambda)^\mu \times (-1)^{1+\mu+\lambda}\gamma_\lambda(r_1 r_2), \tag{16}$$

the magnetic interaction term D'' can be written

$$D''=\sum_{\lambda=0}^{\infty}\sum_{\mu=\lambda-1}^{\mu=\lambda+1}(-1)^{j_1+j_2'+J+\lambda+\mu}\begin{Bmatrix} j_1' & j_2' & J \\ j_2 & j_1 & \mu \end{Bmatrix}\delta_{JJ'}\delta_{MM'}$$
$$\times\int_0^\infty\int_0^\infty r_1^2 r_2^2\gamma_\lambda(r_1r_2)(j_1'\|(\vec{\alpha}_1\times C_1^\lambda)^\mu\|j_1)(j_2'\|(\vec{\alpha}_2\times C_2^\lambda)^\mu\|j_2)\,dr_1\,dr_2\,. \tag{17}$$

The reduced matrix element $(j'\|(\vec{\alpha}\times C^\lambda)^\mu\|j)$ is given by

$$(j'\|(\alpha\times C^\lambda)^\mu\|j)=\frac{i}{r^2}[\mu,j,j']^{1/2}\Pi(l'\lambda+1\ l)\Bigg[(-1)^l\sqrt{2}\begin{pmatrix}1&\lambda&\mu\\-1&0&1\end{pmatrix}\begin{pmatrix}j'&j&\mu\\-\frac{1}{2}&-\frac{1}{2}&1\end{pmatrix}(F'G+G'F)$$
$$+(-1)^{j+1/2}\begin{pmatrix}1&\lambda&\mu\\0&0&0\end{pmatrix}\begin{pmatrix}j'&j&\mu\\-\frac{1}{2}&\frac{1}{2}&0\end{pmatrix}(G'F-F'G)\Bigg]\,. \tag{18}$$

Some algebra, involving 3-j symbols, the analytic expressions for some special 3-j symbols,[16] and the recursion relation among the magnetic quantum numbers, leads to

$$D''=\sum_{\lambda=0}^{\infty}(-1)^{j_2+j_2'+J}[j_1,j_1',j_2,j_2']^{1/2}\begin{Bmatrix} j_1' & j_2' & J \\ j_2 & j_1 & \lambda \end{Bmatrix}\begin{pmatrix}j_1'&j_1&\lambda\\-\frac{1}{2}&\frac{1}{2}&0\end{pmatrix}\begin{pmatrix}j_2'&j_2&\lambda\\-\frac{1}{2}&\frac{1}{2}&0\end{pmatrix}\delta_{JJ'}\delta_{MM'}$$
$$\times\Bigg[\Bigg(\frac{\lambda}{2\lambda-1}\langle P_{11}^\lambda\gamma_{\lambda-1}P_{22}^\lambda\rangle+\frac{\lambda+1}{2\lambda+3}\langle Q_{11}^\lambda\gamma_{\lambda+1}Q_{22}^\lambda\rangle\Bigg)\Pi(l_1'\ \lambda\ l_1)\Pi(l_2'\ \lambda\ l_2)-(1-\delta_{\lambda0})\frac{(\kappa_1'+\kappa_1)(\kappa_2'+\kappa_2)}{\lambda(\lambda+1)}$$
$$\times\langle U_{11}\gamma_\lambda U_{22}\rangle\Pi(l_1'\ \lambda+1\ l_1)\Pi(l_2'\ \lambda+1\ l_2)\Bigg]\,, \tag{19}$$

where

$$P_{ij}^\lambda(r)=[(\kappa_j-\kappa_i')/\lambda]U_{ij}(r)+V_{ij}(r)\,, \tag{20}$$
$$Q_{ij}^\lambda(r)=[(\kappa_j-\kappa_i')/(\lambda+1)]U_{ij}(r)-V_{ij}(r)\,, \tag{21}$$
$$U_{ij}(r)=G_i'(r)F_j(r)+F_i'(r)G_j(r)\,, \tag{22}$$
$$V_{ij}(r)=G_i'(r)F_j(r)-F_i'(r)G_j(r)\,. \tag{23}$$

The exchange matrix elements can be obtained by performing the exchange operation $n_1\kappa_1\rightarrow n_2\kappa_2$ (i.e., exchanging the quantities associated with orbital 1 with the quantities associated with orbital 2) on the direct matrix elements [Eqs. (11) and (19)] and multiplying by the phase factor $(-1)^{J-j_1-j_2}$.

The total radiationless transition probability for a transition $n_1'\kappa_1'\rightarrow n_1\kappa_1\,n_2\kappa_2$, in j-j coupling, is

$$T=\tau\,\frac{1}{2j_1'+1}\sum_{\substack{J,J'\\M,M'}}\sum_{\kappa_2'}|D-E|^2\,, \tag{24}$$

where

$$\tau=\begin{cases}\frac{1}{2} & \text{if } n_1\kappa_1=n_2\kappa_2\\ 1 & \text{otherwise}\end{cases}\,. \tag{25}$$

III. NUMERICAL CALCULATIONS

We calculate the Auger matrix elements with Dirac-Hartree-Slater wave functions[17,18] corresponding to the initial state with one inner-shell vacancy. The continuum wave functions are obtained by solving the Dirac-Slater equations with the same atomic potential as for the initial state. With this treatment, the orthogonality of the wave functions is assured, and the approximation is good for all but the lightest elements. Because there are very many possible Auger transitions that can deexcite any given inner-shell vacancy state of a heavy element (about 200 final two-hole configurations in j-j coupling), we use the j-j configuration average energies in the calculations. These average Auger energies were found by using the "$Z+1$ rule" with theoretical neutral-atom binding energies.[18] Comparison with our relativistic Dirac-Hartree-Slater calculations[19] shows that the "$Z+1$ rule" introduces an error of approximately 30 eV out of a few keV. The effect on the Auger matrix elements caused by this error in energy is found to be negligible. Coster-Kronig transitions, on the other hand, involve much smaller transition energies and their rates are exceedingly energy sensitive; we therefore use Coster-Kronig energies from relativistic, relaxed-orbital Dirac-Hartree-Slater calculations.[19] The continuum wave functions are normalized in the asymptotic region by matching with asymptotic Coulomb wave functions.[6,8]

To derive level widths, fluorescence yields, and Coster-Kronig yields, we combine the Auger and Coster-Kronig rates from the present work with relativistic x-ray transition rates.[20]

TABLE I. L_2-subshell Auger and Coster-Kronig widths and total widths (in eV), Coster-Kronig, and fluorescence yields.

Element	$\Gamma_A(L_2)$	$\Gamma_{23}(L_2)$	$\Gamma(L_2)$	f_{23}	ω_2
$_{70}$Yb	2.662	0.625	4.358	0.143	0.246
$_{74}$W	2.753	0.671	4.821	0.139	0.290
$_{80}$Hg	2.877	0.725	5.696	0.127	0.368
$_{88}$Ra	3.028	0.797	7.243	0.110	0.472
$_{90}$Th	3.060	0.814	7.712	0.106	0.498
$_{92}$U	3.082	1.186	8.620	0.138	0.505
$_{96}$Cm	3.126	2.260	10.708	0.211	0.497

IV. RESULTS AND DISCUSSION

The L_2 Auger and Coster-Kronig rates were calculated for seven elements in the range $70 \leq Z \leq 96$. Results are listed in Table I. Transitions that fill L_1- and L_3-subshell vacancies were calculated for three elements (Table II).

For comparison with previous relativistic calculations,[6,8] the K-LL Auger rates for Hg were also computed; our results agree to better than 4% with the earlier work.[6,8]

Some of the L-shell Coster-Kronig and Auger rates for different j-j configurations are compared with the results of nonrelativistic calculations[21-23] in Fig. 1. One finds that relativistic effects are small in some types of transitions, e.g., for L_3-M_3M_5, L_2-L_3N_5, and L_1-L_3N_4 rates. In some other transitions, by contrast, relativistic effects substantially alter the rates; thus the L_2-M_4M_5 rate at $Z=80$ is reduced by ~30% if relativity is taken into account. A similar disparity in the effects of relativity on K-LL rates has already been noticed.[24]

The total L-subshell Auger widths derived from the present relativistic Dirac-Hartree-Slater (DHS) calculations are compared with nonrelativistic results in Fig. 2. Relativistic effects are seen to reduce L_1 and L_2 Auger widths by 24% and 13%, respectively, and to increase the L_3 Auger width by ~10%, at $Z=80$.

The theoretical L_1- and L_2-subshell fluorescence yields are compared with experimental values[25] in Fig. 3, and the L_2 Coster-Kronig yields f_{23} are shown in Fig. 4. The L_2 Coster-Kronig transitions

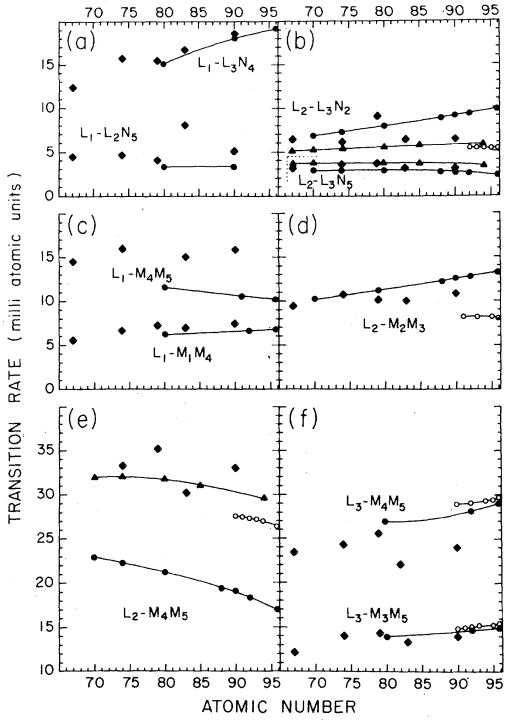

FIG. 1. L-subshell Coster-Kronig and Auger rates, in milliatomic units (1 ma.u. = 0.027 21 eV/$\hbar$ = 4.134 $\times 10^{13}$ sec^{-1}), as functions of atomic number. Results of the present relativistic Dirac-Hartree-Slater calculations are indicated by solid circles; the nonrelativistic rates calculated by McGuire (Refs. 3 and 21) are represented by diamonds; nonrelativistic results of Chen and Crasemann based on the Green-Sellin-Zachor independent-particle model (Ref. 22) are shown as triangles; nonrelativistic Hartree-Fock-Slater results of Chen and Crasemann (Ref. 23) are indicated by open circles.

in the range $90 \leq Z \leq 96$ deserve special attention, because the onset of the strong L_2-$L_3M_{4,5}$ transitions occurs in this region. In our present calculations, both of these transitions are energetically forbidden at $Z=90$. At $Z=92$ and 93, L_2-L_3M_4 transitions are energetically impossible, while L_2-L_3M_5 transitions are allowed with energies of 89.6 and 184.0 eV, respectively. At $Z=94$, both types of transitions are energetically possible, with energies of 86.7 and 294 eV.[19] McGuire[21] has

TABLE II. L_1- and L_3-subshell Auger and Coster-Kronig widths and total widths (in eV), Coster-Kronig and fluorescence yields.

Element	$\Gamma_A(L_1)$	$\Gamma_{12}(L_1)$	$\Gamma_{13}(L_1)$	$\Gamma(L_1)$	f_{12}	f_{13}	ω_1	$\Gamma_A(L_3)$	$\Gamma(L_3)$	ω_3
$_{80}$Hg	2.086	0.992	10.203	14.471	0.069	0.705	0.082	3.878	5.704	0.320
$_{92}$U	2.359	0.846	10.838	16.514	0.051	0.656	0.150	4.571	8.204	0.443
$_{96}$Cm	2.445	0.794	10.644	16.929	0.047	0.629	0.180	4.805	9.189	0.477

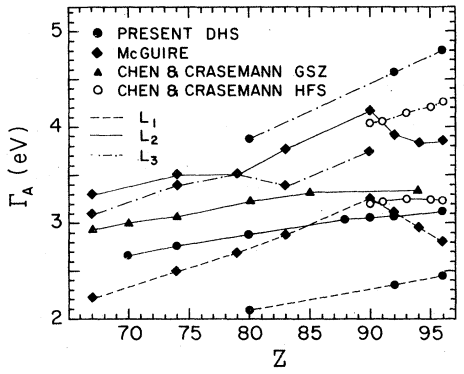

FIG. 2. Total L-subshell Auger widths $\Gamma_A(L_i)$, in eV, as functions of atomic number Z. The present Dirac-Hartree-Slater (DHS) results are compared with nonrelativistic values calculated by McGuire (Refs. 3 and 21) and by Chen and Crasemann on the basis of the Green-Sellin-Zachor (GSZ) independent-particle model (Ref. 22) and from Hartree-Fock-Slater (HFS) wave functions (Ref. 23).

given two values each for f_{23}, ω_2, and $\Gamma(L_2)$ at $Z = 92$ and 94, one set of results including the L_2-L_3M_4 transition, the other excluding it (Figs. 3 and 4). Our theoretical f_{23} for $Z = 94$ (Fig. 4) is obtained by interpolating the L_2 Auger width and the L_2 Coster-Kronig rates (except for L_2-L_3M_4) between $Z = 92$ and $Z = 96$, and using the L_2-L_3M_4 transition rate for $Z = 96$. This procedure is justified because the L_2-L_3M_5 rate changes slowly between $Z = 92$ and $Z = 96$ (from 13.45 to 12.57 ma.u.). It is apparent from Figs. 3 and 4 that our present DHS calculations agree well with experiment,[25] while the nonrelativistic theoretical values[21] of f_{23} agree poorly above $Z = 90$.

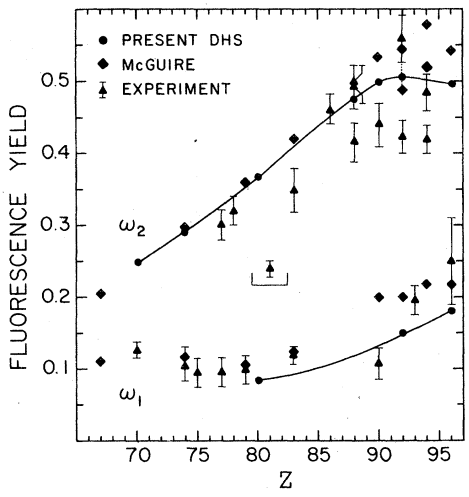

FIG. 3. L_1-subshell fluorescence yields ω_1 and L_2 fluorescence yields ω_2, as functions of atomic number Z. Results from the present relativistic (DHS) calculations are compared with those from nonrelativistic calculations of McGuire (Refs. 3 and 21); the latter comprise two values each for $Z = 92$ and 94, one including and one excluding the L_2-L_3M_4 transition (see text). Experimental results compiled by Krause (Ref. 25) are also shown.

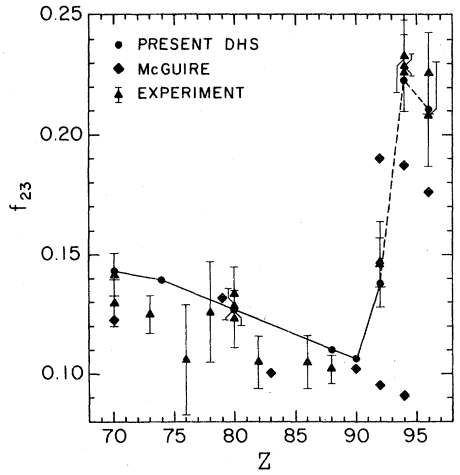

FIG. 4. Coster-Kronig yields f_{23} (as defined in Ref. 2) plotted against atomic number Z. The present relativistic (DHS) values are compared with nonrelativistic results of McGuire (Ref. 21); the latter comprise two yields each for $Z = 92$ and 94, one including and one excluding the L_2-L_3M_4 transition (see text). Experimental values compiled by Krause (Ref. 25) are also shown.

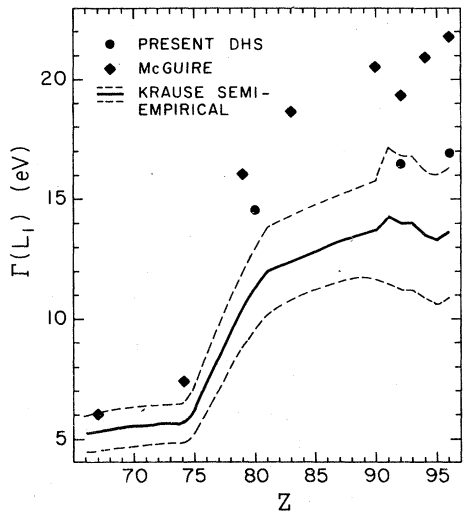

FIG. 5. Total widths $\Gamma(L_1)$ of L_1-subshell vacancy states, in eV, as a function of atomic number Z. The present relativistic (DHS) calculations are compared with nonrelativistic results of McGuire (Ref. 21) and with the semiempirical level widths of Krause and Oliver (Ref. 26) (solid curve, with error limits indicated by broken lines).

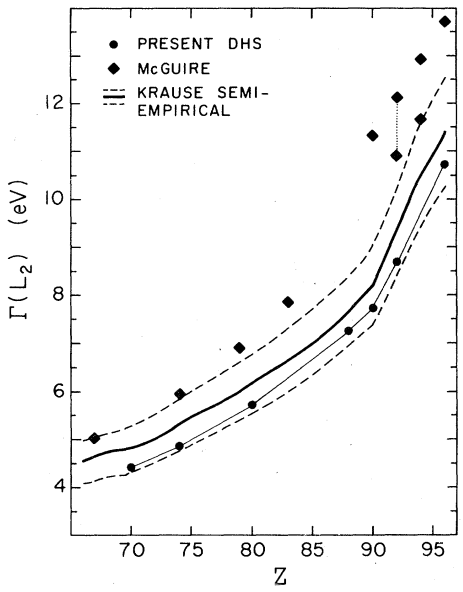

FIG. 6. Total widths $\Gamma(L_2)$ of L_2-subshell vacancy states, in eV, as a function of atomic number Z. The present relativistic (DHS) results are compared with those of nonrelativistic calculations by McGuire (Ref. 21). The latter include two values for $Z=92$ and 94, one with and one without the L_2-L_3M_4 transition (see text). Semiempirical level widths of Krause and Oliver (Ref. 26) are also shown (solid curve with error limits indicated by broken lines).

Theoretical L-subshell level widths were derived by adding Scofield's relativistic x-ray widths[20] to our total Auger and Coster-Kronig widths (Figs. 5 and 6). The L level widths found in this manner agree to within 10% with Krause's semiempirical results,[26] while nonrelativistic theoretical L_1 and L_2 widths[21] are consistently larger than the semiempirical results (e.g., by 40% for L_2 and 50% for L_1 at $Z=90$.

V. CONCLUSIONS

L-subshell Auger and Coster-Kronig transition rates have been calculated relativistically with Dirac-Hartree-Slater wave functions, for selected elements in the range $70 \leq Z \leq 96$.

When atomic properties that depend on outer orbitals are calculated, the effect of relativity tends to arise primarily from the wave functions, which differ from nonrelativistic wave functions because the potential is produced by an atomic electron distribution that is drawn more toward the nucleus than in the nonrelativistic approximation.[27] In the inner-shell processes calculated in the present paper, on the other hand, the relativistic aspects of the interaction V_{12} in the matrix elements [Eqs. (2) and (3)] also play a significant role. Thus the term $(\vec{\alpha}_1 \cdot \vec{\alpha}_2)\exp(i\omega r_{12})/r_{12}$ [Eq. (4)] contributes on the order of 10% as much to the matrix elements as the retarded Coulomb term $\exp(i\omega r_{12})/r_{12}$.

The effect of relativity on the L-shell radiationless transitions is found to be important; it affects the L-subshell Auger widths by 10%-25% and individual transition rates to various final j-j configurations by as much as 40% at $Z=80$. The L-subshell level widths and L_2 Coster-Kronig yields f_{23} from the present work agree much better than nonrelativistic theoretical values with semiempirical and experimental results.

ACKNOWLEDGMENTS

We thank K.-N. Huang for his contributions in the early stages of this research. This work was supported in part by the U. S. Army Research Office (Grant No. DAAG29-78-G-0010), by the National Aeronautics and Space Administration (Grant No. NGR 38-003-036), and by the Air Force Office of Scientific Research (Grant No. 79-0026).

[1]G. Wentzel, Z. Phys. 43, 524 (1927).
[2]W. Bambynek, B. Crasemann, R. W. Fink, H.-U. Freund, H. Mark, C. D. Swift, R. E. Price, and P. Venugopala Rao, Rev. Mod. Phys. 44, 716 (1972).
[3]E. J. McGuire, in *Atomic Inner-Shell Processes*, edited by B. Crasemann (Academic, New York, 1975), Vol. I, p. 293.
[4]M. H. Chen and B. Crasemann, Phys. Rev. A 12, 959 (1975).
[5]H. S. W. Massey and E. H. S. Burhop, Proc. R. Soc. Ser. A 153, 661 (1936).
[6]W. N. Asaad, Proc. R. Soc. A 249, 555 (1959).
[7]M. A. Listengarten, Izv. Akad. Nauk SSR, Ser. Fiz. 25, 803 (1961); 26, 182 (1962) [Bull. Acad. Sci. USSR, Phys. Ser. 25, 803 (1961); 26, 182 (1962)].
[8]C. P. Bhalla, J. Phys. B 3, L9 (1970); Phys. Rev. A 2, 722 (1970); J. Phys. B 3, 916 (1970); C. P. Bhalla and D. J. Ramsdale, *ibid.* 3, L14 (1970).
[9]D. Chattarji and B. Talukdar, Phys. Rev. 174, 44 (1968).
[10]C. Møller, Ann. Phys. (Leipzig) 14, 531 (1932).
[11]A. I. Akhiezer and V. B. Berestetskii, *Quantum Electrodynamics* (Wiley, New York, 1965).
[12]K.-N. Huang, J. Phys. B 11, 787 (1978).
[13]J. B. Mann and W. R. Johnson, Phys. Rev. A 4, 41 (1971).
[14]M. E. Rose, *Relativistic Electron Theory* (Wiley, New York, 1961).
[15]A. de-Shalit and I. Talmi, *Nuclear Shell Theory* (Academic, New York, 1963).
[16]M. Rotenberg, R. Bivins, N. Metropolis, and K. Wooten, Jr., *The 3j and 6j Symbols* (MIT, Cambridge, Mass., 1959). There are misprints in Eq. (1.48) of this work.
[17]D. A. Liberman, D. T. Cromer, and J. T. Waber,

Comput. Phys. Commun. 2, 107 (1971).
[18]K.-N. Huang, M. Aoyagi, M. H. Chen, B. Crasemann, and H. Mark, At. Data Nucl. Data Tables 18, 243 (1976).
[19]M. H. Chen, B. Crasemann, K.-N. Huang, M. Aoyagi, and H. Mark, At. Data Nucl. Data Tables 19, 97 (1977).
[20]J. H. Scofield, Phys. Rev. A 10, 1507 (1974); At. Data Nucl. Data Tables 14, 121 (1974).
[21]E. J. McGuire, Phys. Rev. A 3, 587 (1971); *Proceedings of the International Conference on Inner-Shell Ionization Phenomena and Future Applications*, edited by R. W. Fink, S. T. Manson, J. M. Palms, and P. V. Rao [U. S. Atomic Energy Commission Report No. CONF-720404, 1973 (unpublished)], Vol. I, p. 662.
[22]M. H. Chen and B. Crasemann, in *Proceedings of the International Conference on Inner-Shell Ionization Phenomena and Future Applications*, edited by R. W. Fink, S. T. Manson, J. M. Palms, and P. V. Rao [U.S. Atomic Energy Commission Report No. CONF-720404, 1973 (unpublished)], Vol. I, p. 43.
[23]M. H. Chen and B. Crasemann (unpublished).
[24]M. H. Chen and B. Crasemann, Phys. Rev. A 8, 7 (1973).
[25]M. O. Krause (unpublished).
[26]M. O. Krause and J. H. Oliver (unpublished).
[27]J. P. Desclaux and Y.-K. Kim, J. Phys. B 8, 1177 (1975).